QUARTERLY JOURNAL OF THE ROYAL METEOROLOGICAL SOCIETY
Q. J. R. Meteorol. Soc. **135**: 1003–1019 (2009)
Published online 5 May 2009 in Wiley InterScience
(www.interscience.wiley.com) DOI: 10.1002/qj.415

Intercomparison of model simulations of mixed-phase clouds observed during the ARM Mixed-Phase Arctic Cloud Experiment. II: Multilayer cloud

Hugh Morrison,[a]* Renata B. McCoy,[b] Stephen A. Klein,[b] Shaocheng Xie,[b] Yali Luo,[g] Alexander Avramov,[c] Mingxuan Chen,[d] Jason N. S. Cole,[j] Michael Falk,[q] Michael J. Foster,[p] Anthony D. Del Genio,[m,†] Jerry Y. Harrington,[c] Corinna Hoose,[i] Marat F. Khairoutdinov,[e] Vincent E. Larson,[q] Xiaohong Liu,[f] Greg M. McFarquhar,[r] Michael R. Poellot,[v] Knut von Salzen,[w] Ben J. Shipway,[o,‡] Matthew D. Shupe,[s] Yogesh C. Sud,[l,†] David D. Turner,[t] Dana E. Veron,[n] Gregory K. Walker,[l,†] Zhien Wang,[u] Audrey B. Wolf,[m] Kuan-Man Xu,[h,†] Fanglin Yang[k] and Gong Zhang[r]

[a]*National Center for Atmospheric Research, Boulder, Colorado, USA;* [b]*Lawrence Livermore National Laboratory, Livermore, California, USA;* [c]*The Pennsylvania State University, University Park, PA, USA;* [d]*Colorado State University, Fort Collins, CO, USA;* [e]*State University of New York at Stony Brook, Stony Brook, NY, USA;* [f]*Pacific Northwest National Laboratory, Richland, Washington, USA;* [g]*State Key Laboratory of Severe Weather, Chinese Academy of Meterological Sciences, Beijing, China;* [h]*NASA Langley Research Center, Hampton, Virginia, USA;* [i]*ETH Zurich, Institute for Atmospheric and Climate Science, Zurich, Switzerland;* [j]*University of British Columbia, Vancouver, BC, Canada;* [k]*National Centers for Environmental Prediction, Camp Springs, Maryland, USA;* [l]*NASA Goddard Space Flight Center, Greenbelt, Maryland, USA;* [m]*NASA Goddard Institute for Space Studies, New York, NY, USA;* [n]*University of Delaware, Newark, DE, USA;* [o]*Met Office, Exeter, United Kingdom;* [p]*Rutgers University, New Brunswick, New Jersey, USA;* [q]*University of Wisconsin – Milwaukee, Milwaukee, WI, USA;* [r]*University of Illinois, Urbana, IL, USA;* [s]*Cooperative Institute for Research in Environmental Sciences, University of Colorado/NOAA, Boulder, CO, USA;* [t]*University of Wisconsin – Madison, Madison, WI, USA;* [u]*University of Wyoming, Laramie, WY, USA;* [v]*University of North Dakota, Grand Forks, ND, USA;* [w]*Canadian Center for Climate, Vancouver, British Columbia, Canada*

ABSTRACT: Results are presented from an intercomparison of single-column and cloud-resolving model simulations of a deep, multilayered, mixed-phase cloud system observed during the Atmospheric Radiation Measurement (ARM) Mixed-Phase Arctic Cloud Experiment. This cloud system was associated with strong surface turbulent sensible and latent heat fluxes as cold air flowed over the open Arctic Ocean, combined with a low pressure system that supplied moisture at mid-levels. The simulations, performed by 13 single-column and 4 cloud-resolving models, generally overestimate liquid water path and strongly underestimate ice water path, although there is a large spread among models. This finding is in contrast with results for the single-layer, low-level mixed-phase stratocumulus case in Part I, as well as previous studies of shallow mixed-phase Arctic clouds, that showed an underprediction of liquid water path. These results suggest important differences in the ability of models to simulate deeper Arctic mixed-phase clouds versus the shallow, single-layered mixed-phase clouds in Part I. The observed liquid-ice mass ratios were much smaller than in Part I, despite the similarity of cloud temperatures. Thus, models employing microphysics schemes with temperature-based partitioning of cloud liquid and ice masses are not able to produce results consistent with observations for both cases. Models with more sophisticated, two-moment treatment of cloud microphysics produce a somewhat smaller liquid water path closer to observations. Cloud-resolving models tend to produce a larger cloud fraction than single-column models. The liquid water path and cloud fraction have a large impact on the cloud radiative forcing at the surface, which is dominated by long-wave flux. Copyright © 2009 Royal Meteorological Society

KEY WORDS mixed-phase cloud; Arctic clouds; single-column models; cloud-resolving models

Received 5 March 2008; Revised 23 February 2009; Accepted 2 March 2009

1. Introduction

Observations during the 1997–1998 Surface Heat Budget of the Arctic Ocean experiment (SHEBA) showed that when mixed-phase clouds were present, they consisted of a single liquid layer slightly more than half of the time (Shupe *et al.*, 2006). However, deeper mixed-phase cloud systems containing multiple, distinct layers of liquid were also common. These clouds may be similar to the multilayered, liquid-phase stratus that commonly occurs in the Arctic during summer (Jayaweera and

*Correspondence to: H. Morrison, National Center for Atmospheric Research, Boulder, Colorado, 80307, USA. E-mail: morrison@ucar.edu
†The contributions of Anthony D. Del Genio, Yogesh C. Sud, Gregory K. Walker, and Kuan-Man Xu to this article were prepared as part of their official duties as United States Federal Government employees.
‡The contribution of Ben J. Shipway was written in the course of his employment at the Met Office, UK and is published with the permission of the Controller of HMSO and the Queen's Printer for Scotland.

Copyright © 2009 Royal Meteorological Society

Ohtake, 1973; Herman and Goody, 1976; Tsay and Jayaweera, 1984; Curry, 1986; Curry *et al.*, 1988). Several theories have attempted to explain this multiple layering (see the review in Curry *et al.* (1996) for details), but it is unclear which mechanism(s) may be most important. Multilayer, mixed-phase clouds have also been observed in midlatitudes (Fleishauer *et al.*, 2002).

Few studies have focused on multilayered, mixed-phase stratus despite their fairly common occurrence in the Arctic. Presumably, some of the mechanisms proposed to explain multilayered liquid clouds may also pertain to multilayered mixed-phase clouds. However, the presence of ice complicates the picture. Ice crystals falling from upper layers can seed the lower layers, depleting liquid water through riming and the Bergeron–Findeisen process (preferential vapour depositional growth of ice at the expense of liquid due to the lower ice saturation vapour pressure). The sublimation of crystals falling into dry layers may also impact the local static stability. Under some conditions this can result in a decoupling of well-mixed layers from each other and between the lower layer and the surface, and can promote the formation of a secondary, lower-level cloud layer (Harrington *et al.*, 1999).

To further our understanding of Arctic mixed-phase cloud processes and provide a detailed observational dataset for model evaluation, the Mixed-Phase Arctic Cloud Experiment (M-PACE: Verlinde *et al.*, 2007) was recently conducted over northern Alaska and the adjacent Arctic Ocean during September–October 2004. This study compares simulations of mixed-phase clouds observed during M-PACE using several single-column, cloud-resolving, and large-eddy models. Part I of the study (Klein *et al.*, 2009; hereafter Part I) examines model results for a single-layer mixed-phase cloud. The current paper, part two of this study, describes results for a deeper, multilayered, mixed-phase cloud system. The goals are to document the current state of model simulations of Arctic mixed-phase clouds and to suggest future areas of work which the GEWEX Cloud System Study (GCSS) (Randall *et al.*, 2003; GEWEX is the Global Energy and Water Experiment) Polar Cloud Working Group may use to understand model differences and develop recommendations for parametrizations in large-scale models. Part II of this study represents, to our knowledge, the first model intercomparison focused specifically on deep, multilayered mixed-phase clouds which commonly occur in the Arctic. Herein, the approach is taken to subject each model to the same initial condition and advective tendencies of the large-scale circulation as was done in previous model intercomparison studies performed under the auspices of the GCSS. Additional discussion of the background and broad motivation for GCSS model intercomparison studies is given in Part I.

The paper is organized as follows. Section 2 gives a case description. Section 3 provides an overview of the instrumentation and observations. Section 4 describes the experimental design. Brief descriptions of the participating models are provided in section 5. Section 6 discusses the baseline model results. Sensitivity tests are described in section 7. Finally, summary and conclusions are given in section 8.

2. Case description

M-PACE was conducted from 27 September through to 22 October over the North Slope of Alaska (NSA) and adjacent Arctic Ocean (Verlinde *et al.*, 2007). M-PACE sought to collect a comprehensive dataset to investigate physical processes in mixed-phase clouds using two research aircraft and a host of ground-based instrumentation. The M-PACE domain consisted of the region bounded by four surface sites: Barrow, Atqasuk, Toolik Lake and Oliktok Point (Figure 1).

In this study, we focus on the multilayered, mixed-phase cloud that was observed during 5–8 October 2004. This cloud system was associated with a rather complex synoptic-scale flow field. An anticyclone to the north of Alaska over the ice-covered central Arctic Ocean brought persistent flow from the east-northeast at low levels with considerable fetch over the open water of the Beaufort Sea. The flow of cold air from the pack ice and over open water drove the formation of boundary layer clouds that advected over the North Slope of Alaska, similar to the low-level, single-layer case described in Part I. However, a small, mid-level low pressure system drifted into the M-PACE domain from the east that also promoted considerable moistening and cloudiness at mid-levels, in contrast to the case in Part I. The time evolution of cloudiness at Barrow (Figure 2) is illustrated by the cloud fraction derived from the Active Remotely-Sensed Cloud Locations (ARSCL) algorithm (Clothiaux *et al.*, 2000).

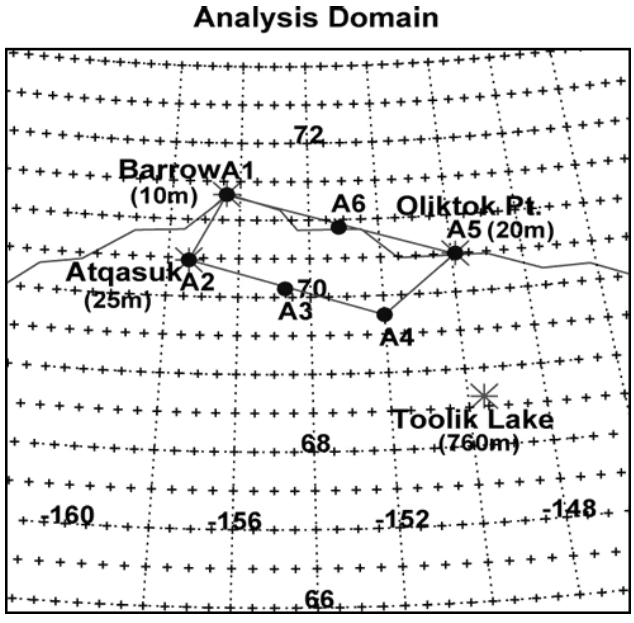

Figure 1. Map of the M-PACE analysis domain (region bounded by A1–A6) and location of the surface observing sites.

Copyright © 2009 Royal Meteorological Society

DOI: 10.1002/qj

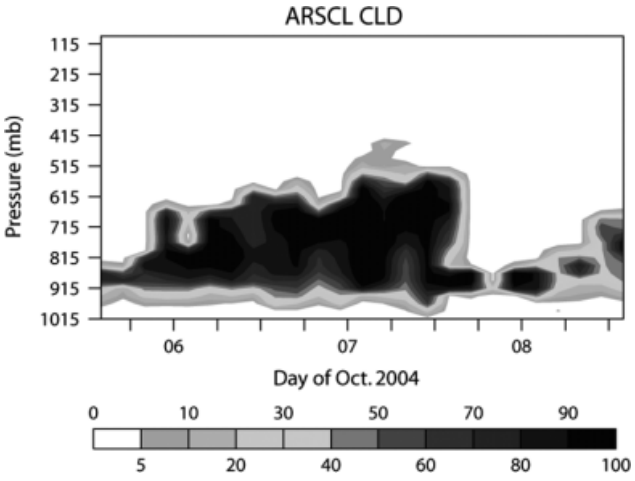

Figure 2. Time–height plot of the ARSCL-derived cloud fraction (%).

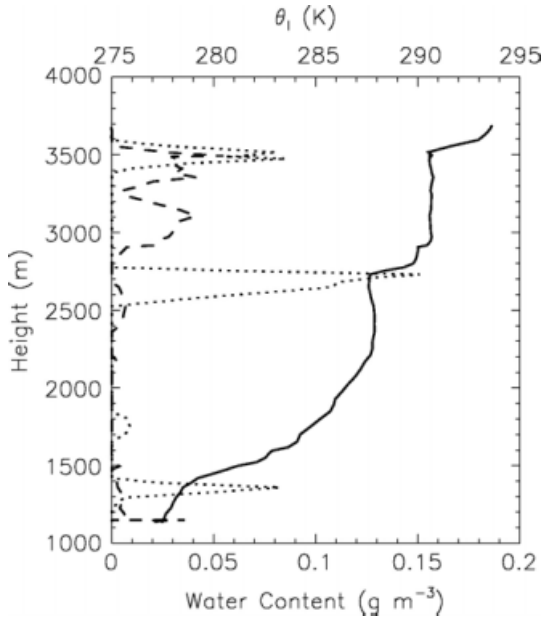

Figure 3. Example of an aircraft profile of liquid water potential temperature, θ_l (solid), liquid water content (dotted), ice water content (dashed), observed during an ascent spiral at about 1917 UTC on 6 October.

The deep, multilayered cloud system on 6 and 7 October consisted of a number of distinct liquid layers with ice crystals falling between the liquid layers as indicated by aircraft measurements (Figure 3). This complex, multilayered cloud structure was also captured by ground-based remote sensing, i.e. the Arctic High Spectral Resolution Lidar (Eloranta, 2005). The ice particles that extended through the depth of the cloud system reached the surface in the form of light snow showers. Interestingly, the liquid layers appeared to be associated with well-mixed layers that were decoupled from each other (indicated by the profile of liquid water potential temperature seen in Figure 3). Elevated well-mixed layers associated with mixed-phase clouds have been previously observed in the Arctic (Pinto, 1998) as well as in midlatitudes (Fleishauer *et al.*, 2002).

3. Observations

The University of North Dakota Citation aircraft, which provided detailed *in situ* microphysical data used in this study, was based at Deadhorse, Alaska, and flew a number of spirals over Barrow and Oliktok Point as well as ramped ascents and descents between the two sites (see Figure 5 in Verlinde *et al.* (2007) for an example of a typical flight pattern). Citation measurements of cloud microphysics (liquid and ice water contents, number concentrations, and effective radii) are described in detail in Part I and references therein. There were three flights (on 5, 6, 8 October) during this case, with a total of about 7.7 flight hours; about 5 flight hours were in clouds and/or precipitation. Most samples were below 2 km, with no samples taken below 400 m.

Ground-based instruments were deployed at the NSA surface sites. These instruments included two-channel microwave radiometer, lidar, and millimetre cloud radar to determine liquid water path (Turner *et al.*, 2007, hereafter TURNER; Wang, 2007, hereafter WANG), profiles of ice water content (Shupe *et al.*, 2006, hereafter SHUPE-TURNER), and cloud occurrence, boundaries, and phase (Wang and Sassen, 2001; Shupe, 2007; WANG). Liquid water path is available from Oliktok Point, Atqasuk, and Barrow, while the other cloud property retrievals are available only for Barrow. Uncertainty estimates are provided in Part I and references therein.

Profiles of temperature, water vapour mixing ratio and horizontal winds were obtained from sounding balloons launched every 6 hours from the four surface sites bounding the M-PACE domain. Surface measurements were only available at Barrow, Atqasuk and Oliktok Point. Surface observations used here to compare with the models include upwelling and downwelling radiative fluxes and precipitation rate.

4. Experimental design

The model specifications for this intercomparison are similar to previous Atmospheric Radiation Measurement (ARM) intercomparison studies for the ARM Southern Great Plains site (Ghan *et al.*, 2000; Xie *et al.*, 2005; Xu *et al.*, 2005), with participation from both single-column models (SCMs, representing a single grid cell of a general-circulation or weather-prediction model), and cloud-resolving models (CRMs). The fairly large domain in the vertical dimension precluded the participation of higher-resolution large-eddy models, although these models did participate in Part I. The simulation period is from 1400 UTC 5 October to 1400 UTC 8 October.

Initial conditions and large-scale forcings used by all participating models are derived from the ARM variational analysis for M-PACE (Xie *et al.*, 2006). Initial profiles are based on the observed areal averages of temperature, water vapour mixing ratio and horizontal wind velocity for the M-PACE region at 25 mb increments in the vertical. Above 215 mb, a standard Arctic profile is applied to the initial fields.

Copyright © 2009 Royal Meteorological Society

DOI: 10.1002/qj

The primary forcing terms in the SCM/CRM governing equations are the large-scale advective tendencies of temperature and water vapour mixing ratio. The large-scale forcings are based on the variational analysis calculated over the four-sided 240 × 100 km grid shown in Figure 1. Large-scale forcings from the variational analysis are calculated between 1015 and 90 mb. Forcings above 90 mb are obtained by interpolation, assuming tendencies of zero at a height of 20 km. The large-scale advective forcings of temperature, $\overline{T}$, and water vapour mixing ratio, $\overline{q}$, are specified using the total (sometimes called 'revealed') advective forcing, defined on isobaric surfaces as

$$\left(\frac{\partial \overline{T}}{\partial t}\right)_{\mathrm{L.S}} \equiv -\mathbf{v}\cdot\nabla\overline{T} - \omega\frac{\partial \overline{T}}{\partial p} + \frac{\omega}{c_p}\alpha, \qquad (1)$$

and

$$\left(\frac{\partial \overline{q}}{\partial t}\right)_{\mathrm{L.S}} \equiv -\mathbf{v}\cdot\nabla\overline{q} - \omega\frac{\partial \overline{q}}{\partial p}, \qquad (2)$$

where p is pressure, ω is the large-scale vertical pressure velocity, c_p is the specific heat of air at constant pressure, $\mathbf{v}$ is the large-scale two-dimensional (2D) wind vector, ∇ is the horizontal del operator, and α is the specific volume of air (the inverse of air density). The advective forcings derived for the period are shown in Figure 4. The large-scale advection of hydrometeors is neglected since these terms were not calculated in the analysis. The profile of large-scale horizontal wind is also derived from the variational analysis. The models were asked to maintain this large-scale wind profile in whatever way they saw fit (most models used nudging).

The lower surface is treated as land, ignoring the small fraction of the domain seen in Figure 1 which is over ocean. Although there is some uncertainty given that the lower part of the cloud system advected from the open ocean, where surface fluxes were presumably larger than over land, we chose this model domain for consistency with the large-scale forcing from the variational analysis. Time-varying values of surface turbulent latent and sensible heat fluxes and surface temperature are specified from the analysis. The time-averaged (between 0000 UTC 6 October and 1400 UTC 8 October) latent and sensible turbulent surface heat fluxes are 18 and 2 W m^{-2} respectively, while the surface skin temperature is −1.6°C. Note that the specified surface temperature is used here only for radiative transfer calculations; it is not directly coupled to the modelled atmosphere via the turbulent heat fluxes. Broadband visible albedo is specified at 0.85, corresponding with the snow-covered land surface. The treatment of radiation in the models is described in more detail in section 4 of Part I.

Although there was day-to-day variability in the aerosol characteristics as indicated by measurements at the National Oceanic and Atmospheric Administration/Earth System Research Laboratory (NOAA/ESRL) Global Monitoring Division observatory located near Barrow (as well as inferred from variability in the aircraft droplet concentration measurements), pristine conditions and low aerosol loading was encountered during this case as well as the single-layer case in Part I. For simplicity, we use the same aerosol and ice nuclei specifications as were used for the single-layer case (see Part I for details).

5. Model descriptions

Thirteen SCMs and four CRMs participated in the intercomparison for this case-study. The SCMs include one operational weather prediction model (NCEP); five operational climate models (CCCMA, ECHAM, GFDL, GISS, SCAM3); and four models used primarily for research (ARCSCM, MCRAS, SCRIPPS, UWM). In addition, there are three models that were developed by modifying the base models to include a two-moment cloud microphysics scheme, i.e. a scheme that predicts both mixing ratios and number concentrations of the hydrometeor species (MCRASI, SCAM3-LIU, SCAM3-MG). The number of vertical levels is shown in Table I, and ranges from 16 to 64.

Among the CRMs, two models are two-dimensional (UCLA-LARC, RAMS-CSU), and two are three-dimensional (SAM, METO). Horizontal resolution varies from 500 m (SAM, METO) to 1 km (RAMS-CSU) to 2 km (UCLA-LARC), with a domain size of about 60 to 250 km in the relevant horizontal dimension(s). The number of vertical levels in the baseline simulations ranges from 45 to 52 (see Table I). For model details, including references, see Tables I and II in Part I. Note that spatial resolution of some of the models differs here relative to

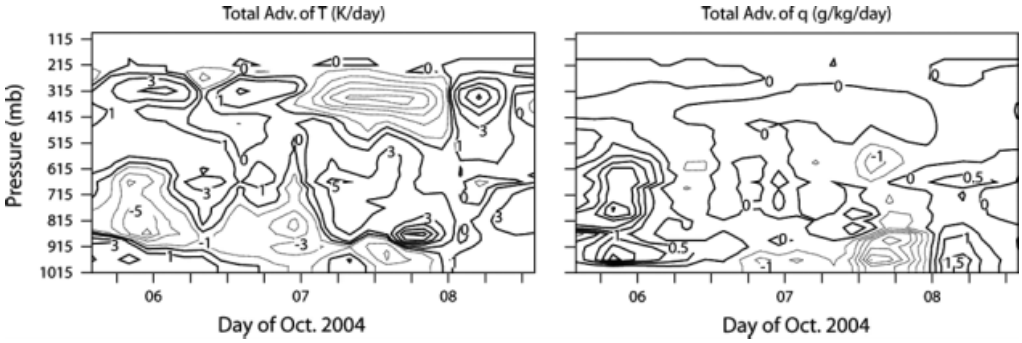

Figure 4. Time–height plot of the large-scale total advective tendencies of temperature and water vapour mixing ratio.

Copyright © 2009 Royal Meteorological Society

DOI: 10.1002/qj

Table I. Number of vertical levels in the participating models for both the baseline and sensitivity simulation with increased vertical resolution.

Model name	Model type	Number of levels – Baseline	Number of levels – Sensitivity
ARCSCM	SCM	30	59
CCCMA	SCM	35	50
ECHAM	SCM	31	98
GFDL	SCM	24	96
GISS	SCM	35	–
McRAS	SCM	17	137
McRASI	SCM	17	137
NCEP	SCM	64	640
SCAM3	SCM	26	60
SCAM3-MG	SCM	26	–
SCAM3-LIU	SCM	26	60
SCRIPPS	SCM	20	53
UWM	SCM	100	500
RAMS-CSU	CRM	52	71
SAM	CRM	45	69
UCLA-LARC	CRM	45	99
METO	CRM	45	81

that shown in Tables I and II in Part I; furthermore, not all of the models in Part I participated here.

Given that microphysics may be a key in simulating mixed-phase clouds, its treatment in the models is described in more detail in Part I. The parametrizations of microphysics can be classified into three broad categories which span a wide range of complexity (see Part I for details). All microphysics schemes in the models participating in this case use the bulk approach (prediction of bulk properties of the hydrometeor species such as mass mixing ratio, with an assumption of the underlying shape of the particle size distributions). There are no models here that use the bin approach (explicit prediction of the hydrometeor size distributions), although bin models did participate in Part I. The three types of bulk parametrizations are (1) 'single-moment schemes with T-dependent partitioning' (MCRAS, NCEP, SAM, SCAM3), i.e. schemes that include a single prognostic variable for cloud water and partition liquid and ice according to temperature; (2) 'single-moment schemes with independent liquid and ice' (CCCMA, GFDL, GISS, SCRIPPS, UWM), i.e. schemes that include separate prognostic variables for liquid and ice; (3) 'double-moment schemes' (ARCSCM, ECHAM, MCRASI, METO, RAMS-CSU, SCAM3-LIU, SCAM3-MG, UCLA-LARC), i.e. schemes that include prognostic variables for both mixing ratios and number concentrations of cloud liquid and/or ice. Hereafter '1-M' and '2-M' will refer to all single-moment and double-moment microphysics schemes, respectively.

The SCAM3 microphysics includes separate prognostic variables for cloud liquid and ice mixing ratios, but the fraction of liquid and ice is repartitioned each time step according to temperature. For the case here, UWM used the microphysics scheme of Long (2003) instead of Larson *et al.* (2006) as in Part I.

In general, only the models with two-moment microphysics represent the dependence of cloud properties on aerosols. However, one of the models with two-moment microphysics does not have an explicit dependence of cloud properties on aerosol (METO). Furthermore, not all models altered their default aerosol to that recommended in the intercomparison specifications. Thus, we do not focus on representation of cloud–aerosol interactions in this study. None of the models allowed two-way interaction between clouds and aerosols, except for RAMS-CSU, which allowed depletion of ice nuclei after nucleation and subsequent removal. A more detailed description of the various treatments of ice microphysics and ice nucleation is given in Part I.

6. Baseline results

Simulations are compared for the period from 0000 UTC 6 October to 1400 UTC 8 October, which allows for 10 hours of model spin-up time. First, we compare results for the baseline simulations, and then we compare sensitivity tests with either higher vertical resolution or neglect of ice microphysics. The focus is on key cloud and thermodynamic properties that impact the cloud radiative forcing. Thus, we pay particular attention to the cloud liquid water path (which dominates the cloud ice water path in nearly all of the models), as well as the cloud fraction. The analysis is generally based on time-average results, although the modelled and observed cloud properties exhibit significant temporal variability over the period of interest as discussed below. This variability is in contrast with the single-layer case in Part I.

6.1. Cloud morphology

All of the models capture the general evolution of the cloud morphology during the period. An exception is that most of the models produce ice clouds between 300 and 500 mb during the latter part of 7 October and first part of 8 October, which were not observed (see Figure 2). These ice clouds appear to be associated with possibly spurious upper-level vertical motion and cold advection in the large-scale forcing data (see Figure 4). A sensitivity test using ARCSCM with this upper-level cloud suppressed, results in an increase in the instantaneous value of liquid-water path (LWP) by up to a factor of two, mostly due to the increased cloud-top radiative cooling of mid-level mixed-phase clouds. The impact in other models is uncertain without additional sensitivity tests; however, overall it is likely to be small since the appearance of this spurious cloud was brief ($\sim$12 h) relative to the total length of the period.

Interestingly, nearly all of the models produce at least some of the multilayered, mixed-phase cloud structure, with the exception of SAM. Here, the number of liquid layers occurring in the vertical is determined using a

Copyright © 2009 Royal Meteorological Society

DOI: 10.1002/qj

threshold cloud liquid water mixing ratio of 0.01 g kg^{-1}, and a minimum separation distance of 50 m between the layers (note that for the CRMs, the number of layers was calculated using horizontally-averaged data). This suggests that the overall occurrence of multilayering in the simulations is more dependent on the large-scale atmospheric and surface forcing than details of the cloud microphysics or other aspects of the model physics. This finding is consistent with the model sensitivity study of Luo *et al.* (2008), who found that the lower cloud layer was primarily driven by the surface turbulent heat fluxes, while the upper cloud layer was initially formed by large-scale advection and vertical motion, and subsequently maintained by cloud-top radiative cooling. A few of the models here also produce persistent interior mixed-phase layers between the upper and lower layers (CCCMA, GISS); without further sensitivity studies, the mechanism(s) producing these layers is less clear.

Although nearly all of the models produce some multilayering of cloud liquid water, the number of mixed-phase cloud layers (averaged over 0000 UTC 6 October to 1400 UTC 8 October) varies substantially among the simulations, from 1.00 in SAM to 3.10 in CCCMA. Thus, while the overall occurrence of multilayering appears to be dependent mostly on the large-scale atmospheric and surface forcing, the actual number of layers depends on the details of the models. Surprisingly, the number of layers does not appear to be correlated with the vertical resolution. The observed time-averaged number of layers determined from ground-based retrievals at Barrow is 1.36, following the method of Wang and Sassen (2001). The presence of three or more layers occurred less than 10% of the time during this period (see Table II in Luo *et al.*, 2008). Thus, interior mixed-phase layers occurring between the upper and lower layers were rather infrequent. However, we note that the number of layers may be somewhat underestimated due to retrieval uncertainty, which is estimated to be about 0.1 in terms of the time-averaged value.

6.2. Cloud/hydrometeor fraction

Vertical profiles of the observed (ARSCL-derived) cloud/hydrometeor fraction and modelled cloud fraction, averaged over the period 0000 UTC 6 October to 1400 UTC 8 October, are shown in Figure 5. Note that the ARSCL observations do not include precipitation below the base of the lowest cloud layer, while they do include ice precipitation between mixed-phase cloud layers. All CRMs were asked to compute cloud fraction as the fraction of grid volumes with cloud droplet mixing ratios greater than a threshold of 0.01 g kg^{-1} or cloud ice mixing ratios greater than 0.0001 g kg^{-1}. Thus, individual grid cells have a cloud fraction of either 0 or 1 depending on the presence of cloud condensate exceeding these threshold values. The domain-average cloud fraction at a given level is then calculated by averaging the cloud fraction of each grid cell of the CRM at that level. For SCMs, cloud fraction is an inherent property of the model, meant to represent the horizontal fraction of a grid cell that is saturated and contains cloud water or ice.

Compared to the observations, all of the models produce too much cloud above 400 mb. This is related to the spurious production of ice clouds on 7 and 8 October described previously. The median cloud fraction of the CRMs is larger (by about 10–30%) compared to the median of the SCMs. However, it is important to note that there is a large spread among both the CRMs and SCMs, indicated by the range and inner 50% of the model values shown in Figure 5(a). Furthermore, there may be some sensitivity to the condensate thresholds used here to define a 'cloud' in the CRMs. Nonetheless, differences in cloud fraction between the SCMs and CRMs appear to be significant and have an impact on the surface radiative fluxes as described later in this section.

The hydrometeor fraction (cloud and precipitation) is similarly larger for the CRMs than the SCMs, although the median hydrometeor fraction of the CRMs is larger than the ARSCL-derived observations (not shown). The hydrometeor fraction has less relevance to the cloud

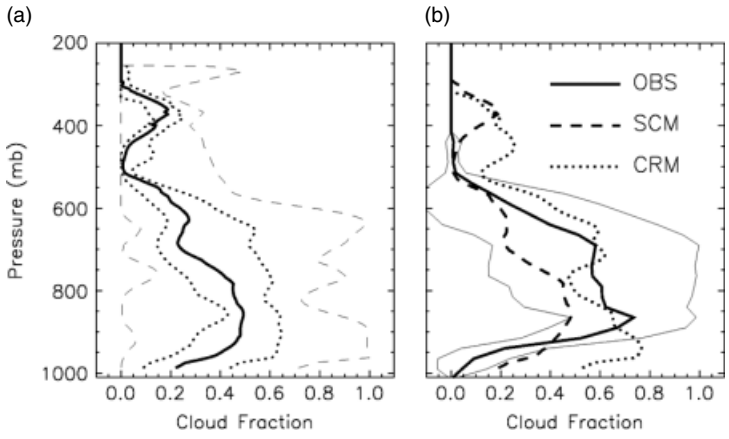

Figure 5. Time-averaged cloud fraction from observations and models as a function of height. The properties depicted are (a) the median of the models (solid line), the inner 50% (dotted line), and the min/max (dashed line); (b) the ARSCL observations (thick solid line with thin solid line indicated +/−1 standard deviation) and median of the SCMs and CRMs. The averaging period is from 0000 UTC 6 October to 1400 UTC 8 October.

Copyright © 2009 Royal Meteorological Society

DOI: 10.1002/qj

radiative forcing in models because they typically neglect the radiative impact of precipitation particles.

6.3. Liquid and ice water contents

Although all of the models produce a mostly overcast, precipitating mixed-phase clouds system, substantial differences exist in the predicted phase partitioning and cloud water and ice amounts. There is a large spread among the modelled cloud liquid water content (LWC) profiles averaged between 0000 UTC 6 October and 1400 UTC 14 October, indicated by the range and inner 50% model values in Figure 6(a). Here the LWC is an in-cloud value, found by dividing the reported grid-mean value by the cloud fraction (since the contribution of rain is small relative to cloud droplets in terms of the total liquid water content in all models, it is neglected). The median values for the CRMs are smaller than the median for the SCMs. However, the cloud fraction produced by the SCMs tends to be smaller than that of the CRMs; thus, the SCM and CRM median liquid water paths are similar as described in section 6.5. Models with one-moment microphysics schemes tend to produce larger liquid water content, especially below 850 mb, relative to models with two-moment schemes (not shown). Aircraft observations are also shown in Figure 6(b). These values are in-cloud averages over the three flights that took place during the period (5, 6, 8 October). There is significant variability within flights and especially between the flights, as indicated by the large standard deviation. The aircraft LWCs tend to be similar to the median SCM values but are larger than the CRM median values. However, the aircraft sampled the cloud only over open ocean while the models treated the surface as land; thus, it is not surprising that the modelled clouds contain less water. In contrast, the modelled values of liquid water path (LWP) are larger than the ground-based retrievals as described below.

Because the observations (both from the aircraft and radar retrievals) do not distinguish between cloud and precipitation ice, the models must include both cloud and precipitation ice (snow and graupel) for a consistent comparison (note that in many models precipitation ice is a significant fraction of the total ice). In models with bulk microphysics, the partitioning between cloud and precipitation ice is rather arbitrary, despite the fact that this issue is important since models typically only include radiative effects of the cloud ice. In some of the SCM simulations, precipitation ice contents were not reported (ECHAM, GISS, MCRAS, MCRASI, NCEP, SCRIPPS). These models are therefore not included in the comparison with the observed ice-water content (IWC).

There is little difference in the median values of IWC for the SCMs and CRMs, although there is a large spread among the individual models (Figure 7(a)). The model median IWC profile is similar to the aircraft observations and radar retrievals in terms of its distribution with height (i.e. the decrease of IWC with greater height), although the model values are consistently smaller by a factor of 2–3 (Figure 7(b)). The radar-derived and aircraft profiles of IWC are similar (generally within a factor of two throughout the vertical), although there is considerable temporal variability associated with both values. However, the variability of IWC between aircraft flights is less than it is for the LWC. Some of the differences between the aircraft and retrieved IWC may result from sampling by aircraft over ocean versus ground-based retrievals over land, in addition to retrieval and measurement uncertainties.

6.4. Hydrometeor number concentrations and effective radii

The aircraft-observed droplet concentrations are generally between 10 and 40 cm^{-3}, and do not exhibit any clear trend with height (see Fig. 11 in Luo *et al.*, 2008). The average droplet effective radius is between 8 and 13 μm. The aircraft-observed crystal concentrations (for particles larger than 53 μm) have significant variability over time and height, with average concentrations for each flight generally less than 10 L^{-1}, although on 8 October the mean concentration in the lower part of the cloud exceeded 80 L^{-1} (see Fig. 13 in Luo *et al.*, 2008). The

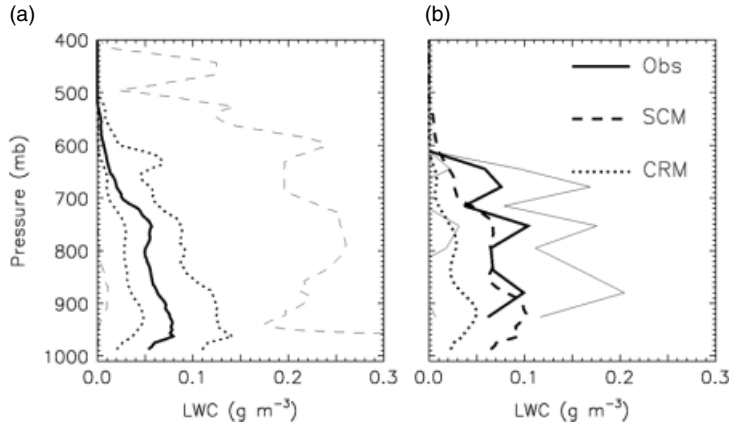

Figure 6. Time-averaged in-cloud liquid water content from observations and models as a function of height. The properties depicted are (a) the median of the models (solid line), the inner 50% (dotted line), and the min/max (dashed line); (b) the aircraft observations (thick solid line with thin solid line indicating +/−1 s.d.) and median of the SCMs and CRMs. The averaging period is from 0000 UTC 6 October to 1400 UTC 8 October for the simulations. The aircraft value is the average of three flights that occurred on 5, 6 and 8 October.

Copyright © 2009 Royal Meteorological Society

DOI: 10.1002/qj

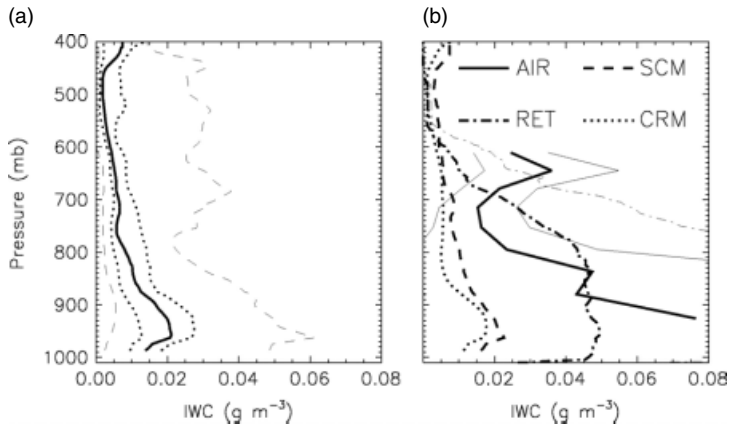

Figure 7. Time-averaged in-cloud ice water content from observations and models as a function of height. The properties depicted are (a) median of the models (solid line), the inner 50% (dotted line), and the min/max (dashed line); (b) the aircraft observations 'AIR' (thick solid line with thin solid line indicating $+/-1$ s.d.), SHUPE-TURNER radar retrievals 'RET' (thick dot-dash line with thin dot-dash line indicating $+/-1$ s.d.), and median of the SCMs and CRMs. The averaging period is from 0000 UTC 6 October to 1400 UTC 8 October for the simulations and radar retrievals. The aircraft value is the average of three flights that occurred on 5, 6 and 8 October.

average ice effective radius is between 23 and 26 μm and is fairly constant with height. The model median mass-weighted effective radii of liquid and ice are 9 and 68 μm, respectively, and the model median mass-weighted number concentrations of liquid and ice are 51 cm^{-3} and 1.4 L^{-1}, respectively. These are similar to the values reported for the single-layer case in Part I. However, general conclusions about the consistency of models with these hydrometeor observations cannot be made due to the very wide range of model results, especially for the ice microphysics, from the approximately 50% of models that submitted the relevant diagnostics. Much of this inter-model variability is the result of models coupling with different aerosol characteristics. For models that did couple with M-PACE aerosol (ARCSCM, UCLA-LARC, ECHAM), the droplet number concentrations and effective radii are similar to observations, generally ranging between 10 to 50 cm^{-3} and 8 to 15 μm, respectively. However, there is no evidence that coupling with M-PACE aerosol produces better overall simulation in terms of liquid and ice water paths, cloud fraction, cloud radiative forcing, etc. A similar conclusion was reached for the single-layer case in Part I. For ice, the number concentration (cloud ice plus snow) and effective radius vary widely even among the simulations that were coupled with the observed ice nucleus concentrations (see Part I for a detailed description of the various treatments of ice nucleation). Previous studies have shown strong sensitivity of LWP to the ice particle number concentration in simulated Arctic mixed-phase clouds (Harrington *et al.*, 1999; Jiang *et al.*, 2000; Morrison *et al.*, 2003; Prenni *et al.*, 2007). Here there is no significant trend between modelled ice particle concentrations and LWP; there was also significant scatter in this relationship in Part I.

6.5. Liquid and ice water paths

The retrieved domain-average liquid and ice water paths, averaged from 0000 UTC 6 October to 1400 UTC 8 October, are shown in Table II. The modelled values are shown in Table III. The retrieved and modelled time-average values of LWP as a function of the ice water path (IWP) are shown in Figure 8. Uncertainty in the retrieved LWP is illustrated by the range of values using different retrieval method and measurement locations (see Table II). Nonetheless, inter-model differences far exceed the retrieval uncertainty; there is approximately a factor-of-ten spread in average LWP among the models. Ten of the seventeen models produce a time-average LWP larger than the mean retrieved value, with the median model value somewhat larger than retrieved.

Table II. Retrieved liquid water path (LWP) and ice water path (IWP) from ground-based remote sensing, averaged during the period 0000 UTC 6 October to 1400 UTC 8 October.

Retrieval method	Location	LWP (g m^{-2})	IWP (g m^{-2})
WANG	Barrow	121	–
WANG	Oliktok Point	119	–
TURNER/ TURNER-SHUPE	Barrow	116	81
TURNER	Oliktok Point	58	–
TURNER	Atqasuk	55	–

The median LWP for models with two-moment microphysics is somewhat smaller than the median for models with one-moment microphysics (both single-moment with T-dependent partitioning and with independent liquid and ice). Thus, models with two-moment microphysics tend to produce a mean LWP that is slightly closer to the retrieved values (although there is considerable scatter). This point is reinforced by the simulations which use different microphysics schemes in otherwise the same model; there is a reduced LWP produced by the two-moment schemes of SCAM3-LIU and SCAM3-MG relative to SCAM3 which employs a one-moment scheme (155 and 136 versus 298 g m^{-2}), and MCRASI relative to MCRAS (44 versus 83 g m^{-2}). There is little difference

Copyright © 2009 Royal Meteorological Society

DOI: 10.1002/qj

Table III. Modelled liquid water path (LWP) and ice water path (IWP) for the baseline and sensitivity tests with no ice microphysics and increased vertical resolution. '1-M T-dep', '1-M Ind', and '2-M' refer to the models using 1-moment microphysics schemes with T-dependent partitioning, one-moment schemes with independent liquid and ice, and two-moment schemes, respectively. Asterisk (*) indicates models that did not include precipitation ice. Median IWP values are derived only from models that include both cloud and precipitation ice.

Model/Ensemble	LWP (g m^{-2})			IWP (g m^{-2})	
	Baseline	High vert. resolution	No ice	Baseline	High vert. resolution
Median model	123	125	332	42	43
Median SCM	123	121	452	42	48
Median CRM	126	128	230	38	34
Median 1-M T-dep	147	127	332	48	49
Median 1-M Ind	123	172	693	42	63
Median 2-M	115	117	230	27	26
ARCSCM	199	197	452	28	26
CCCMA	182	220	216	62	83
ECHAM	93	166	97	1.9*	1.7*
GFDL	65	102	717	42	42
GISS	109	–	–	37*	–
McRAS	83	128	332	3.5*	4.5*
McRASI	44	81	504	5.8*	18*
NCEP	30	27	87	36*	34*
SCAM3	298	334	–	42	55
SCAM3-MG	136	–	–	21	–
SCAM3-LIU	155	105	–	87	121
SCRIPPS	245	162	668	20*	22*
UWM	123	103	1448	36	31
RAMS-CSU	170	184	215	13	20
SAM	211	125	793	54	43
UCLA-LARC	82	117	245	49	51
METO	26	20	180	26	25

in median LWP between the SCMs and CRMs. However, the UCLA-LARC CRM has a smaller LWP compared to the ARCSCM SCM (82 versus 199 g m^{-2}), even though both models use the same two-moment microphysics scheme.

In contrast to the LWP, the models tend to strongly underpredict IWP relative to the radar retrievals (even considering only those models that include both cloud and precipitation ice). On the face of it, this suggests too little conversion of liquid to cloud and/or precipitating ice. However, biases in the LWP and IWP may also be independent of one another (such as too slow conversion of cloud liquid to rain leading to positive bias in LWP, combined with too fast sedimentation of ice leading to negative bias in IWP); without additional sensitivity tests that are beyond the scope of this paper it is not possible to quantify which individual processes (microphysical or otherwise) impact the biases and spread of model results. Models with two-moment microphysics schemes tend to produce smaller IWP than those with one-moment schemes, resulting in an even more substantial underprediction of IWP relative to the retrieved value. It should be kept in mind that there is considerable uncertainty in the retrieved IWP; the model median IWP (considering only models that include cloud and precipitation ice) is at the limit of the factor-of-two estimate of uncertainty in the retrieved value. There is considerable spread of IWP among the models, although much of this difference is due to the exclusion of precipitation ice in some of the models. For models that include both cloud and precipitation ice, there is still a factor-of-five spread in the IWP, but this is less than the spread of LWP among the same models. In these models, the cloud IWP is less than 20% of the total IWP (i.e. including cloud ice, snow and graupel), with a few exceptions (ARCSCM, CCCMA, SAM, UCLA-LARC). Similar to Part I, nearly all of the precipitating ice mass is represented by snow rather than graupel in the models that include both species.

Time series of the modelled median and retrieved LWP and total IWP are shown in Figure 9. For median IWP, only the models that reported both cloud and precipitation ice are included. The overprediction of LWP and underprediction of IWP seen in the time-averages occurs primarily on 6 October and the first half of 7 October, when deeper clouds extending to mid-levels predominated in the real atmosphere (see Figure 2). During the brief period at the end of 7 October and first

Copyright © 2009 Royal Meteorological Society

DOI: 10.1002/qj

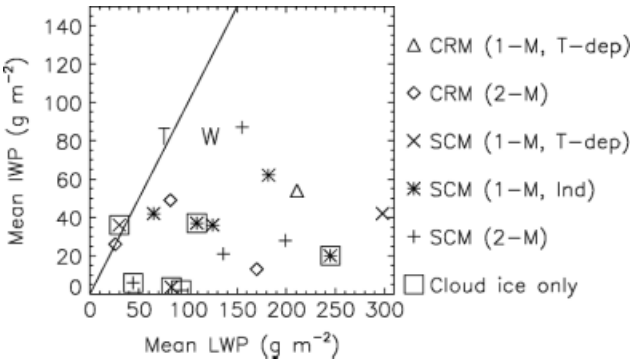

Figure 8. Time-averaged ice water path (IWP) as a function of liquid water path (LWP) for the models and ground-based retrievals. Symbols plotted for each model indicate type (SCM versus CRM) and cloud microphysics scheme (one-moment with *T*-dependent partitioning '1-M, T-dep', one-moment with independent liquid and ice '1-M, Ind', and two-moment '2-M'). 'Cloud ice only' indicates the models that did not report precipitation ice. 'T' and 'W' indicate LWP retrievals using the TURNER method averaged between Barrow, Oliktok, and Atqasuk, and WANG method averaged between Barrow and Oliktok, respectively, and retrieved IWP using the SHUPE-TURNER method at Barrow. The solid line indicates 1:1 ratio of LWP and IWP.

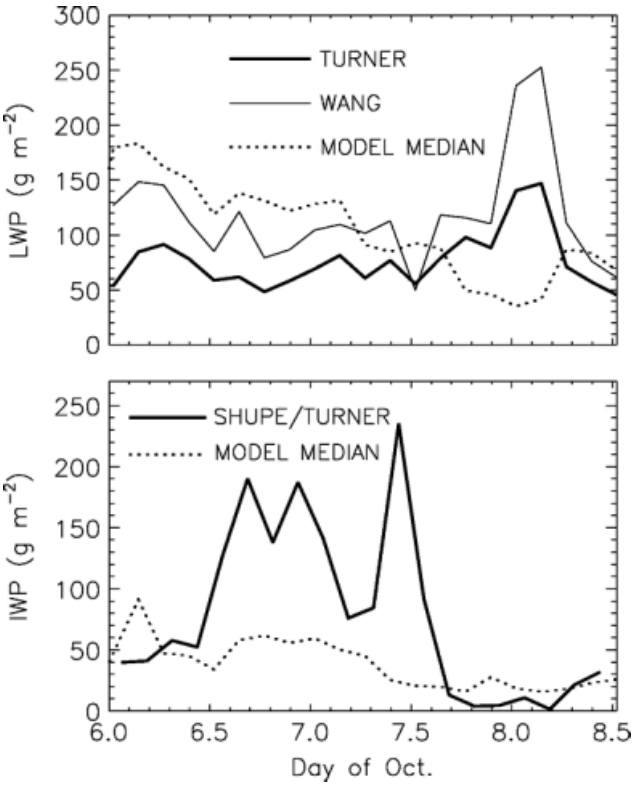

Figure 9. Time series of liquid water path (LWP) and ice water path (IWP) for the median model values and ground-based retrievals. Retrieved LWP is calculated using the WANG method averaged between Barrow and Oliktok Point and the TURNER method averaged between Barrow, Oliktok Point, and Atqasuk. Retrieved IWP is calculated using the SHUPE-TURNER method at Barrow.

few hours on 8 October, when a single-layer, low-level cloud was observed, the models underestimate LWP and overestimate IWP, consistent with results for the single-layer case in Part I. Some of this underestimate of LWP may be caused by reduced cloud-top radiative cooling of the low- and mid-level cloud due to the spurious upper-level ice cloud that was produced at this time in nearly all of the simulations as described previously. In the observations, the transition from a deep, multilayer cloud to low-level single-layer cloud at the end of 7 October was marked by sharply increasing LWP and decreasing IWP to values similar to the low-level cloud in Part I. This suggests that the absence of seeding from above and increased cloud-top radiative cooling of the low-level cloud may have increased LWP during this brief period. The roles of seeding and cloud-top radiative cooling are also inferred from sensitivity tests of the case described by Luo *et al.* (2008). They found that cloud-top radiative cooling was critical for maintaining liquid water in the mid-level cloud, although turning off the ice microphysics (including seeding from above) had a comparatively greater role than radiative cooling for the lower layer mixed-phase cloud.

6.6. Surface precipitation

Ice fell to the surface intermittently during the period in the form of light snow. Unfortunately, quantitative estimates of the surface snow rate are highly uncertain due to factors such as blowing snow and because of the small precipitation amounts. The National Weather Service station in Barrow recorded an average precipitation rate of 0.7 mm/day; however, the ARM precipitation rate measured at Barrow was a factor of seven larger. The total precipitation rate in the simulations, averaged from 0000 UTC 6 October to 1400 UTC 8 October, varies widely, with the largest value of 1.62 mm/day in ECHAM and the smallest value of 0.34 mm/day in CCCMA. Most of the models produced primarily frozen precipitation (snow), but in several simulations the majority of the surface precipitation was liquid (ECHAM, SCAM3, SCAM3-LIU, MCRAS, MCRASI, RAMS-CSU, NCEP). Most of the models that produced primarily rain at the surface (with the exception of RAMS-CSU) did so because they diagnose the precipitation phase based on a threshold temperature of 0°C; near-surface temperatures were slightly above freezing in these simulations.

6.7. Thermodynamic profiles

Inter-model differences in the temperature, averaged between 0000 UTC 6 October and 1400 UTC 14 October, are rather small (maximum of ∼5 K over the depth of the profile) (Figure 10). The median values for the different model ensembles are close to observations (within 2 K), with the CRM median slightly colder than the SCM median. Inter-model differences in the time-average water vapour mixing ratio profiles are also small (maximum of ∼0.6 g/kg over the depth of the profile) (Figure 11). The median values for different model ensembles are close to observations (within 0.3 g/kg), with the CRM median value slightly drier between 600 and 900 mb compared to the SCM median, consistent with the slightly colder median temperature. The spread among models and error relative to observations for the temperature and water vapour profiles are considerably less than previous model

Copyright © 2009 Royal Meteorological Society

DOI: 10.1002/qj

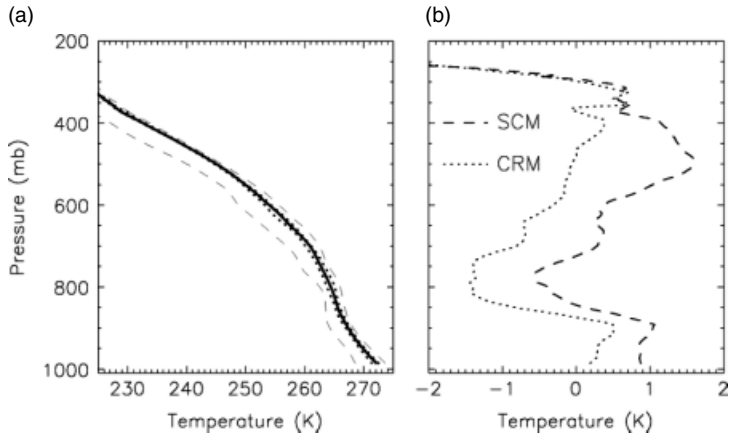

Figure 10. Time-averaged temperature from the models as a function of height. The properties depicted are (a) the median of the models (solid line), the inner 50% (dotted line), and the min/max (dashed line); (b) difference of the median value of the SCMs and CRMs from observations derived from ARM variational analysis. The averaging period is from 0000 UTC 6 October to 1400 UTC 8 October.

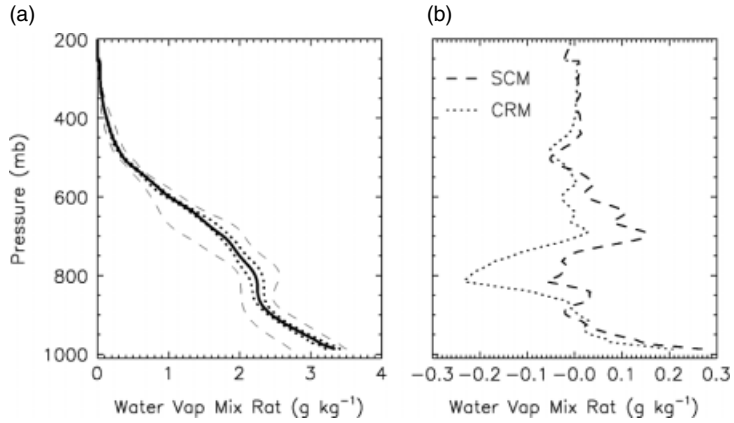

Figure 11. As in Figure 10, except for the water vapour mixing ratio.

intercomparisons of deep and shallow midlatitude frontal clouds (see Fig. 14 in Xie *et al.*, 2005; Fig. 10 in Xu *et al.*, 2005). These results also indicate that the substantial inter-model differences in cloud fraction and condensate amount are not associated with large differences in the thermodynamic profiles.

6.8. Radiative fluxes

In the Arctic, the downward component of the surface radiation is strongly affected by clouds and is an important quantity that affects the surface temperature of land and sea ice. Although this effect is disabled in the model simulations here, it is important to assess whether the modelled clouds have the correct radiative impacts.

Despite the general overprediction of LWP, several models produce a time-average surface downwelling long-wave radiation (LW) flux that is reasonably close to observations (Figure 12). This occurs because the LW flux saturates at a mean LWP greater than about 50–75 g m^{-2}, so that the clouds tend to emit as blackbodies and further increase in condensate amount has little impact (Stephens, 1978). Conversely, models that produce a mean LWP less than 50–75 g m^{-2} underpredict the LW flux. Ice has less impact on downwelling radiative fluxes because of the dominance of cloud water mass relative to cloud ice in nearly all of the models.

The relationship between surface downwelling LW and column cloud fraction is shown in Figure 12(b). Here, column cloud fraction is calculated by assuming maximum overlap in the vertical (note that this overlap assumption is not necessarily employed for radiative calculations in all of the models but is used here for simplicity to illustrate the key points). Not surprisingly, downwelling LW flux increases steadily with greater column cloud fraction. All of the CRMs produce a mean column cloud fraction close to 100%, while the SCMs produce values ranging from 62 to 100%. Several of the SCMs produce a small column cloud fraction (<90%), consistent with the smaller median SCM cloud fraction compared with the median CRM value described previously. These differences in cloud fraction explain much of the inter-model difference in downwelling LW, especially for models that produce a mean LWP exceeding 50–75 g m^{-2}. For example, SCAM3, which has the largest mean LWP of all models, produces one of the smallest mean downwelling LW fluxes because of the relatively low mean column cloud fraction (73%). On the other hand, METO has a column cloud fraction of nearly 100%, but has the second lowest mean downwelling LW flux among all models because

Copyright © 2009 Royal Meteorological Society

DOI: 10.1002/qj

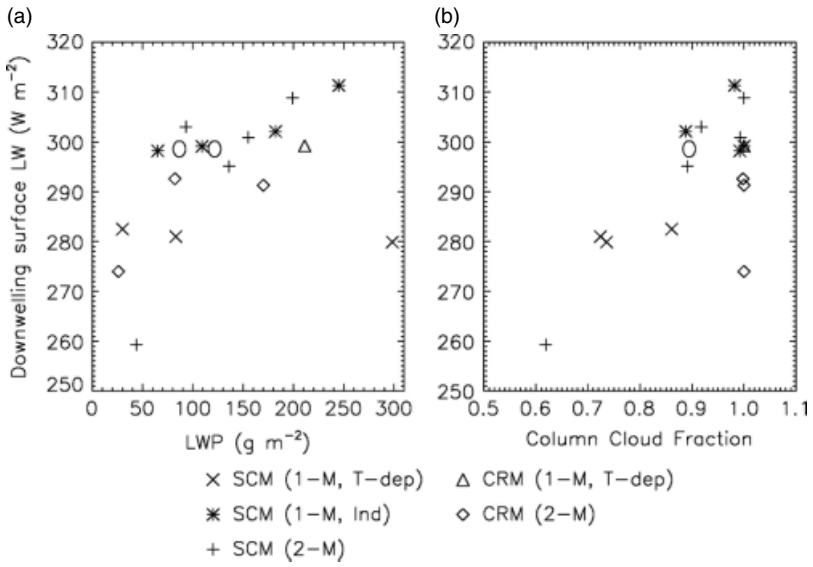

Figure 12. Time-averaged modelled and observed downwelling surface LW flux as a function of (a) the liquid water path (LWP), (b) column cloud fraction. Time averaging is from 0000 UTC 6 October to 1400 UTC 8 October. Symbols plotted for each model indicate type (SCM versus CRM) and cloud microphysics scheme (one-moment with T-dependent partitioning '1-M, T-dep', one-moment with independent liquid and ice '1-M, Ind', and two-moment '2-M'). 'O' indicates observed values.

of the small mean LWP (26 g m^{-2}). These results highlight the importance of both cloud fraction and condensate amount in determining the LW fluxes. Because all of the models produce clouds at low levels and the temperature profiles among the simulations are similar, differences in cloud emission temperature appear to not be as significant in explaining differences in surface LW flux.

The time-averaged downwelling solar radiation (SW) flux at the surface decreases with increasing LWP and column cloud fraction as expected, although there is considerable scatter (Figure 13). The observed SW flux is in the middle range of the model values. Note that for this case the time-average downwelling SW flux is about an order of magnitude smaller than the LW flux due to the high zenith angle and extended periods of darkness. The modelled upwelling top-of-atmosphere (TOA) radiative fluxes also exhibit differences consistent with the column cloud fraction (and less so with the mean LWP), although the spread among models is less for the TOA LW flux than the downwelling surface LW flux (not shown). Nearly all of the models underestimate the LW TOA flux due to the unrealistic presence of upper-level ice clouds on 7 and 8 October.

7. Sensitivity tests

7.1. No ice microphysics

Prior modelling studies have suggested the sensitivity of mixed-phase clouds to representation of ice microphysics (Pinto, 1998; Morrison and Pinto, 2006; Prenni *et al.*, 2007). This sensitivity is examined here with additional simulations in which all ice processes were turned off. All of the models except GISS, SCAM3, SCAM3-LIU and SCAM3-MG ran this test, which allows us to examine the role of ice in depleting liquid water in the simulations.

The average LWP for each model over the period 0000 UTC 6 October to 1400 UTC 8 October for the sensitivity test without ice as a function of the baseline LWP is shown in Figure 14. As expected, LWP increases in the simulations without ice, although this increase is quite small for some models (especially ECHAM which had very little ice in the control simulation). Other models show a substantial increase in LWP without ice microphysics (GISS, METO, MCRASI, UWM). This suggests that the relatively small mean baseline LWP produced by three of these four models (METO, GFDL, MCRASI) is mostly due to their greater depletion of liquid water by ice relative to the other models. The three CRMs with two-moment microphysics (RAMS-CSU, UCLA-LARC, METO) all produce similar LWP without ice microphysics (ranging from 180 to 245 g m^{-2}), even though they differ greatly for the baseline simulations with ice (ranging from 26 to 170 g m^{-2}). Some of the differences in the amount of liquid depleted by ice are directly attributable to differences in the temperature-based partitioning between liquid and ice in the models with the most simplified treatment of the microphysics (NCEP, SAM, SCAM3).

Time-averaged median values of LWP for the ice-free simulations are shown in Table III. In contrast to the baseline results, the CRM median LWP is smaller than the SCM median value in the runs without ice. The median value of the models with two-moment microphysics is less than the value of the models with one-moment microphysics, similar to the baseline simulations. All but four models produce appreciable drizzle at the surface in these simulations (defined as a mean rain rate greater than 0.01 mm d^{-1}). The median model value is

Copyright © 2009 Royal Meteorological Society

DOI: 10.1002/qj

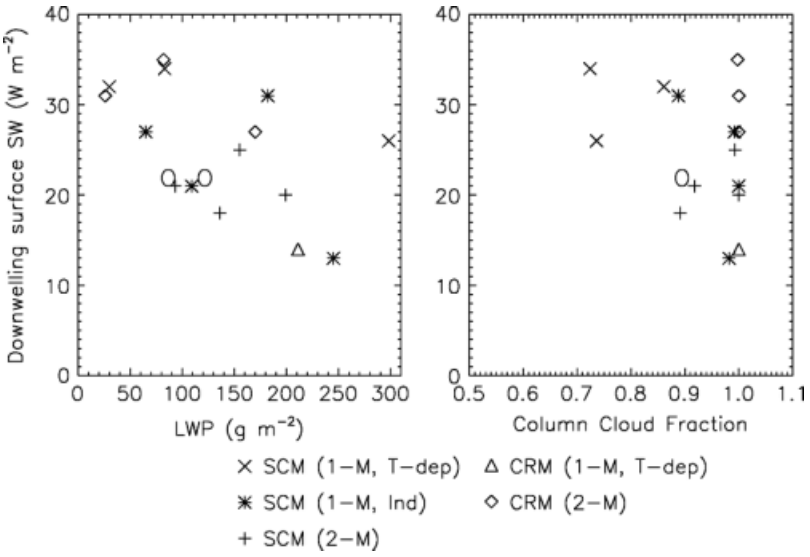

Figure 13. As in Figure 12, but for the downwelling surface SW flux.

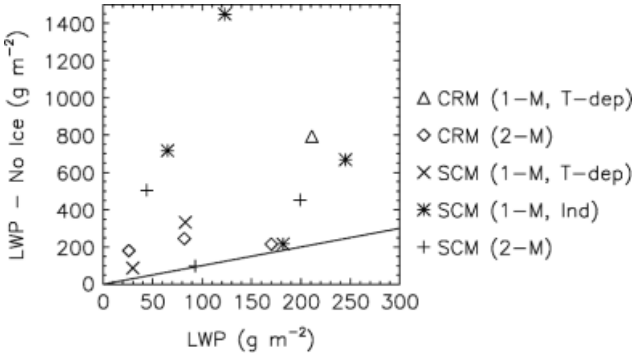

Figure 14. Time-averaged liquid water path (LWP) from the sensitivity simulations with no ice microphysics as a function of the baseline simulated LWP. Time averaging is from 0000 UTC 6 October to 1400 UTC 8 October. Symbols plotted for each model indicate type (SCM versus CRM) and cloud microphysics scheme (one-moment with T-dependent partitioning '1-M, T-dep', one-moment with independent liquid and ice '1-M, Ind', and two-moment '2-M'). The solid line indicates 1:1 ratio of sensitivity to baseline LWP.

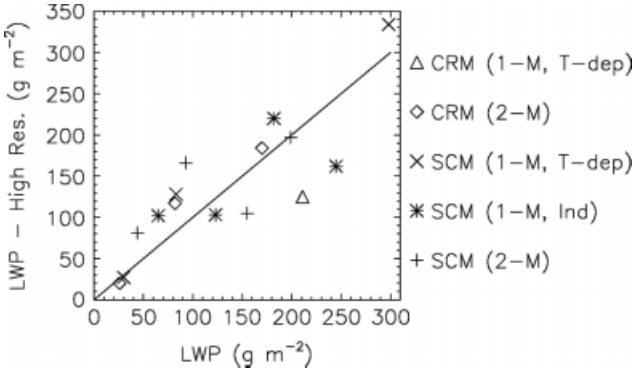

Figure 15. As in Figure 14, except for the sensitivity simulations with increased vertical resolution.

0.024 mm d^{-1} and the maximum model mean rain rate is 0.10 mm d^{-1}.

7.2. Increased vertical resolution

As described in Part I, low vertical resolution in models may lead to non-convergence of simulated cloud properties, especially for the fairly thin mixed-phase layers for this case. To explore this issue, all of the models except for SCAM3-MG and GISS ran sensitivity tests with increased vertical resolution. The participants chose how much to increase the vertical resolution (see Table I).

Figure 15 shows the LWP from the high resolution run, averaged over the period 0000 UTC 6 October to 1400 UTC 8 October, as a function of the average baseline LWP for each model. Values for each model are also shown in Table III. The mean high-resolution LWP is within a factor of two or less of the baseline LWP for all of the models. Interestingly, increasing the resolution leads to an increase in LWP for many of the models that produce smaller LWP for the baseline run; conversely, it leads to a decrease in LWP for many of the models that produce larger baseline LWP. Excluding the models with the simplest treatment of microphysics (single-moment with T-based partitioning of liquid and ice in NCEP, SAM, SCAM3) and the METO outlier, the spread among the models for the high resolution runs is 82 g m^{-2} in MCRASI to 198 g m^{-2} in CCCMA. The same models produce a much larger spread in baseline LWP, ranging from 49 g m^{-2} in MCRASI to 278 g m^{-2} in SCRIPPS. Thus, there is evidence suggesting that increasing the vertical resolution improves the convergence of LWP among models, as long as they have a reasonably sophisticated treatment of the microphysics (at least one-moment with separate treatment of liquid and ice), with the exception of the METO model. In contrast, there were no consistent trends in the high resolution simulations noted for the single-layer case in Part I. In general, the IWP exhibits limited sensitivity to the vertical resolution (with the exception of MCRASI) (see Table III).

Copyright © 2009 Royal Meteorological Society

DOI: 10.1002/qj

Interestingly, the increase in vertical resolution has a limited impact on the macrophysical structure and multilayering of mixed-phase regions (not shown). This finding is consistent with the baseline results that show no consistent trend in terms of multilayering between models with lower and higher vertical resolution.

8. Discussion and conclusions

This modelling study extensively compared simulations from 13 SCMs and 4 CRMs of a case-study of a deep, multilayered, mixed-phase stratiform cloud system observed during M-PACE on 5–8 October 2004. To our knowledge, this is the first such model intercomparison focusing specifically on multilayered mixed-phase clouds that commonly occur in the Arctic. This cloud system formed by surface forcing via large turbulent heat and moisture fluxes over the open ocean combined with a weak, mid-level low pressure system. A unique feature of this case is the presence of multiple liquid layers in the vertical, with ice precipitation falling between the layers and intermittently reaching the surface as light snow.

The models were able to reasonably reproduce the cloud macrophysical structure, consisting of a persistent boundary layer cloud and intermittent mid-level cloudiness, although there were significant inter-model differences in cloud fraction. Nearly all of the models produced unrealistic upper-level ice clouds on 7 and 8 October, which may have resulted from biases in the large-scale forcing. In general, the SCMs produced smaller cloud fraction than the CRMs, in contrast to model results from more strongly-forced cases of shallow and deep midlatitude frontal systems that showed no consistent differences between SCM and CRM cloud fraction (Xie *et al.*, 2005; Xu *et al.*, 2005). However, we also note that these previous studies used larger condensate thresholds to define cloud fraction in the CRMs, which could account for some of the difference. Large inter-model differences in cloud fraction as well as condensate amount were not associated with significant differences in the temperature or water vapour profiles.

All of the models except one were able to produce multiple layers of liquid in the mixed-phase clouds as were observed, suggesting that the occurrence of multilayering was more a result of the large-scale atmospheric and surface forcing than details of the model physics. Although nearly all of the models produced some multilayering, the actual number of layers varied widely among the models and, surprisingly, was not correlated with the vertical resolution. The number of layers was also poorly correlated with other key cloud quantities such as LWP and IWP.

In the Arctic, the downward component of the surface radiation is a critical quantity that affects the surface temperature of land and sea ice (although this effect was not included here). Differences in the cloud fraction were key in producing inter-model variability in the downwelling surface LW fluxes (as well as the SW fluxes, although they were considerably smaller on average than the LW fluxes). Several of the SCMs produced a small column cloud fraction (<90%) and thus small downward LW flux. These results highlight the need for a realistic simulation of cloud fraction in order to produce the correct cloud forcing at the surface in the Arctic. Differences in LWP were comparatively less important for the downwelling LW flux because several of the models produced a mean LWP greater than 50–75 g m^{-2}, meaning that the clouds tended to emit as near-blackbodies. However, LWP had a large impact on the downwelling surface LW fluxes in models with a mean LWP less than 50–75 g m^{-2}. The impact of the cloud ice water path on the radiative fluxes was secondary, since cloud liquid was dominant in nearly all of the models.

The majority of models overpredicted the mean observed LWP, especially relative to the TURNER retrievals, and underpredicted the mean IWP. This finding is in sharp contrast to results from the low-level single-layer case in Part I, as well as previous modelling studies of Arctic mixed-phase stratus that have reported a substantial *underprediction* of LWP by models (Curry *et al.*, 2000; Girard and Curry, 2001; Morrison *et al.*, 2003; Inoue *et al.*, 2006; Morrison and Pinto, 2006; Prenni *et al.*, 2007). Underprediction of LWP was also noted by Xie *et al.* (2005) and Xu *et al.* (2005) in simulations of midlatitude frontal clouds. We note that there is an inconsistency in the lower boundary between Part I (surface treated as ocean) and here (surface treated as mostly land). However, assuming an open ocean surface with larger turbulent heat fluxes here would likely exaggerate the overprediction of LWP. Conversely, assuming a land surface with smaller fluxes in Part I would likely exaggerate the underprediction of LWP found in that study. Thus, our conclusion that the models tend to overpredict LWP here and underpredict it for the single-layer case in Part I is likely not due to the difference in surface conditions.

An analysis of the LWP time series suggested that most of the overprediction of LWP occurred during episodes of deeper cloud that extended into the mid-troposphere. At the end of 7 October and in the first few hours of 8 October, when only a low-level, shallow cloud was present, the models tended to underpredict LWP and overpredict IWP consistent with results from Part I. However, some of this underprediction of LWP may have been due to spurious upper-level ice clouds and reduced cloud-top radiative cooling of the low- and mid-level mixed-phase cloud. The observed LWP (IWP) associated with this low-level, single-layer cloud on 7 and 8 October was much higher (lower) than earlier in the period when deeper clouds predominated. This suggests that the absence of seeding from above as well as stronger cloud-top radiative cooling may have increased LWP when only the single-layer low-level mixed-phase cloud was present.

These results indicate that the models in general behave quite differently for deeper mixed-phase clouds compared to low-level, shallow mixed-phase clouds. In Part I, results suggested that the conversion from liquid to ice was too rapid. The results here seem to suggest the opposite; that is, in general the models were unable to convert

Copyright © 2009 Royal Meteorological Society

DOI: 10.1002/qj

enough liquid to ice. This key difference between the results here and in Part I is potentially explained by the different ice formation mechanisms occurring in shallow, single-layer clouds compared with deeper mixed-phase clouds. In deeper clouds, ice growth via riming and depositional growth may deplete liquid water as crystals fall into the layer ('seeder–feeder' process), while in shallow clouds this process is likely to be much less effective. This was inferred from the observations, as the LWP increased sharply (and IWP decreased sharply) during the transition from deep, multilayered cloud to shallow cloud on 7 October. Thus, models that are able to realistically capture ice formation in one regime may fail in the other. This may be especially true of models with a simple treatment of the microphysics, such as single-moment schemes with temperature-dependent partitioning, since they cannot capture different physical processes that occur at similar temperatures. For example, SCAM3 (employing single-moment microphysics with temperature-dependent partitioning) produced liquid and ice water paths reasonably close to observations in Part I, but significantly over-predicted LWP here owing to the much lower liquid–ice mass ratio that was observed relative to Part I, despite the similarity of cloud temperatures. These results clearly indicate the inadequacy of such temperature-based partitioning of the cloud liquid water and ice in microphysics schemes. Only two models produced reasonable results both here and in Part I (SCAM3-LIU and UCLA-LARC). On the other hand, some of the models with one-moment microphysics schemes (but separate prognostic variables for liquid and ice) produced liquid and ice water paths that were fairly close to observations here but performed poorly in Part I (GFDL, GISS).

Although the models tended to overestimate LWP and underestimate IWP, there were large inter-model differences in both quantities. This variability may have had several major causes. First, there was a large spread among the models in terms of how much cloud liquid water was depleted by the ice. Some of this spread was directly attributable to differences in the temperature-based partitioning between liquid and ice in the models with the most simplified treatment of the microphysics (NCEP, SAM, SCAM3). It is also likely that differences in other parametrizations such as boundary layer may have had a large impact in addition to the treatment of microphysics. The order of magnitude spread in LWP among models here was roughly similar to the spread of LWP found in LES and SCM model intercomparisons of warm marine stratocumulus (Stevens *et al.*, 2005; Zhu *et al.*, 2005), as well as the single-layer mixed-phase case in Part I. Large inter-model differences in the amount of cloud liquid and ice condensate were also noted in simulations of midlatitude frontal clouds (Xie *et al.*, 2005; Xu *et al.*, 2005). Here, increasing the vertical resolution significantly decreased the spread of LWP among those models with a more sophisticated treatment of the microphysics (one-moment with separate treatment of liquid and ice, or two-moment).

Overall, models using two-moment instead of one-moment microphysics schemes produced a somewhat lower LWP that was closer to observations. This difference was even more evident in the simulations without ice, and therefore was not a direct result of differences in the microphysical conversion of liquid to ice. For the low-level single-layer case in Part I, it was found that models with two-moment microphysics schemes tended to produce *greater* amounts of liquid water that were closer to observations than models with one-moment microphysics. Thus, models with two-moment schemes produced results closer to observations in terms of LWP both here and in Part I, even though here they produced less liquid water than models with one-moment schemes, and in Part I they produced more liquid water. However, we emphasize that there is considerable scatter among the simulations; thus, caution is needed when interpreting these results. We also note that here models with one-moment schemes tended to produce larger IWP that was closer to the retrieved value, although the retrieved IWP has considerable uncertainty and the IWP has less impact on the cloud forcing at the surface compared to the LWP. It is possible that some of these differences using one- or two-moment microphysics schemes may be more related to the details of the schemes, rather than more broadly the number of moments predicted. Further explanation for these differences will require additional tests that employ a more constrained framework. As discussed in Part I, one possible route for such tests could involve the comparison of microphysics schemes in the framework of a specified flow field in which radiation and dynamics are non-interactive with the microphysics (Morrison and Grabowski, 2007). Offline tests of individual microphysical processes could also help to further understand differences among the models at the process level.

We emphasize that the generalization of these results to other cases is uncertain. Nevertheless, the availability of this observationally well-constrained case-study, along with that from Part I, adds to the growing number of such datasets and should be valuable for individual modellers to further improve their cloud and cloud microphysics parametrizations.

Acknowledgements

This work is supported by the Office of Science of the United States Department of Energy under grants DE-AI02-94ER61768 (Del Genio), DE-FG02-02ER63337 (McFarquhar), DE-FG02-03ER63539 (Morrison), DE-FG02-05ER64058 (Harrington), DE-FG02-05ER64069 (Wang), DE-FG02-06ER64167 (Turner), DE-FG02-02ER63370 (Chen), DE-FG02-06ER64168 (Poellot), DE-AI02-06ER64183 (Xu and Luo), and DE-FG02-07ER64378 (McFarquhar). M. Chen also is also supported by National Science Foundation grant ATM-0415184. J. Cole is supported by the Canadian Foundation for Climate and Atmospheric Sciences.

Copyright © 2009 Royal Meteorological Society

DOI: 10.1002/qj

M. Falk and V. Larson are supported by National Science Foundation grant ATM-0442605 and sub-award G-7424-1 from the Department of Defense Center for Geosciences/Atmospheric Research at Colorado State University via Cooperative Agreement DAAD19-02-2-0005 with the Army Research Laboratory. C. Hoose is supported by the climate programme of the Swiss National Centre of Competence in Research. Y. Luo is supported by the Chinese Academy of Meteorological Sciences and the United States National Aeronautics and Space Administration's Cloud Modeling and Analysis Initiative. H. Morrison is supported by NASA grant NNG06GBB1G and by the NSF Science and Technology Center for Multi-Scale Modeling of Atmospheric Processes, managed by Colorado State University under cooperative agreement ATM-0425247. The contribution of S. Klein, R. McCoy, and S. Xie to this work is performed under the auspices of the US Department of Energy by Lawrence Livermore National Laboratory under contract DE-AC52-07NA27344. X. Liu acknowledges that the Pacific Northwest National Laboratory is operated for the Department of Energy by Battelle Memorial Institute under contract DE-AC06-76RLO-1830. National Center for Atmospheric Research is sponsored by the National Science Foundation. Comments on the manuscript by R. Pincus and two anonymous reviewers are appreciated.

References

Clothiaux EE, Ackerman TP, Mace GG, Moran KP, Marchand RT, Miller MA, Martner BE. 2000. Objective determination of cloud heights and radar reflectivities using a combination of active remote sensors at the ARM CART sites. *J. Appl. Meteorol.* **39**: 645–665.

Curry JA. 1986. Interactions among turbulence, radiation and microphysics in Arctic stratus clouds. *J. Atmos. Sci.* **43**: 90–106.

Curry JA, Ebert EE, Herman GF. 1988. Mean and turbulent structure of the summertime Arctic cloudy boundary layer. *Q. J. R. Meteorol. Soc.* **114**: 715–746.

Curry JA, Rossow WB, Randall DA, Schramm JL. 1996. Overview of Arctic cloud and radiation characteristics. *J. Climate* **9**: 1731–1764.

Curry JA, Hobbs PV, King MD, Randall DA, Minnis P, Isaac GA, Pinto JO, Uttal T, Bucholtz A, Cripe DG, Gerber H, Fairall CW, Garrett TJ, Hudson J, Intrieri JM, Jakob C, Jensen T, Lawson P, Marcotte D, Nguyen L, Pilewskie P, Rangno A, Rogers DC, Strawbridge KB, Valero FPJ, Williams AG, Wylie D. 2000. FIRE Arctic Clouds Experiment, *Bull. Am. Meteorol. Soc.* **81**: 5–29.

Eloranta EW. 2005. High spectral resolution lidar. Pp 143–163 in *Lidar: Range-resolved optical remote sensing of the atmosphere*, Weitkamp K (ed). Springer-Verlag.

Fleishauer RP, Larson VE, Vonder Haar TH. 2002. Observed microphysical structure of midlevel, mixed-phase clouds. *J. Atmos. Sci.* **59**: 1779–1804.

Ghan SJ, Randall D, Xu K-M, Cederwall R, Cripe D, Hack J, Iacobellis S, Klein SA, Krueger S, Lohmann U, Pedretti J, Robock A, Rotstayn L, Somerville R, Stenchikov G, Sud Y, Walker G, Xie S, Yio J, Zhang M. 2000. A comparison of single column model simulations of summertime midlatitude continental convection. *J. Geophys. Res.* **105**: 2091–2124.

Girard E, Curry JA. 2001. Simulation of Arctic low-level clouds observed during the FIRE Arctic Clouds Experiment using a new bulk microphysics scheme. *J. Geophys. Res.* **106**: 15139–15154.

Harrington JY, Reisin T, Cotton WR, Kreidenweis SM. 1999. Cloud resolving simulations of Arctic stratus. Part II: Transition-season clouds. *Atmos. Res.* **55**: 45–75.

Herman GF, Goody R. 1976. Formation and persistence of summertime Arctic stratus clouds. *J. Atmos. Sci.* **33**: 1537–1553.

Inoue J, Liu J, Pinto JO, Curry JA. 2006. Intercomparison of Arctic regional climate models: Modeling clouds and radiation for SHEBA in May 1998. *J. Climate* **19**: 4167–4178.

Jayaweera K, Ohtake T. 1973. Concentration of ice crystals in Arctic stratus clouds. *J. Rech. Atmos.* **7**: 199–207.

Jiang H, Cotton WR, Pinto JO, Curry JA, Weissbluth MJ. 2000. Cloud resolving simulations of mixed-phase Arctic stratus observed during BASE: Sensitivity to concentration of ice crystals and large-scale heat and moisture advection. *J. Atmos. Sci.* **57**: 2105–2117.

Klein SA, McCoy RB, Morrison H, Ackerman AS, Avramov A, de Boer G, Chen M, Cole JNS, Del Genio AD, Falk M, Foster MJ, Fridland A, Golaz J-C, Hashino T, Harrington JY, Hoose C, Khairoutdinov MF, Larson VE, Liu X, Luo Y, McFarquhar GM, Menon S, Neggers RAJ, Park S, Poellot MR, Schmidt JM, Sednev I, Shipway BJ, Shupe MD, Spangenberg DA, Sud YC, Turner DD, Veron DE, von Salzen K, Walker GK, Wang Z, Wolf AB, Xie S, Xu K-M, Yang F, Zhang G. 2009. Intercomparison of model simulations of mixed-phase clouds observed during the ARM Mixed-Phase Arctic Cloud Experiment. I: Single-layer cloud. *Q. J. R. Meteorol. Soc.* **135**: (in press). DOI:10.1002/qj.416.

Larson VE, Smith AJ, Falk MJ, Kotenberg KE, Golaz J-C. 2006. What determines altocumulus dissipation time? *J. Geophys. Res.* **111**: D19207, DOI:10.1029/2005JD007002.

Long ML. 2003. 'COAMPS® Version 3 Model Description – General Theory and Equations'. NRL Publication NRL/PU/7500-03-448, Technical Information Services Branch, Naval Research Laboratory, Washington, DC.

Luo Y, Xu K-M, Morrison H, McFarquhar GM, Wang Z, Zhang G. 2008. Multi-layer Arctic mixed-phase clouds simulated by a cloud-resolving model: Comparison with ARM observations and sensitivity experiments. *J. Geophys. Res.* **113**: D12208, DOI:10.1029/2007JD009563.

Morrison H, Grabowski WW. 2007. Comparison of bulk and bin warm-rain microphysics models using a kinematic framework. *J. Atmos. Sci.* **64**: 2839–2861.

Morrison H, Pinto JO. 2006. Intercomparison of bulk cloud microphysics schemes in mesoscale simulations of springtime Arctic mixed-phase stratiform clouds. *Mon. Weather Rev.* **134**: 1880–1900.

Morrison H, Shupe MD, Curry JA. 2003. Modeling clouds observed at SHEBA using a bulk parameterization implemented into a single-column model. *J. Geophys. Res.* **108**: 4255, DOI:10.1029/2002JD002229.

Pinto JO. 1998. Autumnal mixed-phase cloudy boundary layers in the Arctic. *J. Atmos. Sci.* **55**: 2016–2038.

Prenni AJ, Harrington JY, Tjernström M, DeMott PJ, Avramov A, Long CN, Kreidenweis SM, Olsson PQ, Verlinde J. 2007. Can ice-nucleating aerosols affect Arctic seasonal climate? *Bull. Am. Meteorol. Soc.* **88**: 541–550.

Randall DA, Krueger S, Bretherton CS, Curry JA, Duynkerke P, Moncrieff M, Ryan B, Starr D, Miller M, Rossow W, Tselioudis G, Wielicki B. 2003. Confronting models with data: The GEWEX Cloud Systems Study. *Bull. Am. Meteorol. Soc.* **84**: 455–469.

Shupe MD. 2007. A ground-based multisensor cloud phase classifier. *Geophys. Res. Lett.* **34**: L22809, DOI:10.1029/2007GL031008.

Shupe MD, Matrosov SY, Uttal T. 2006. Arctic mixed-phase cloud properties derived from surface-based sensors at SHEBA. *J. Atmos. Sci.* **63**: 697–711.

Stephens GL. 1978. Radiation profiles in extended water clouds. II: Parameterization schemes. *J. Atmos. Sci.* **35**: 2123–2132.

Stevens B, Moeng C-H, Ackerman AS, Bretherton CS, Chlond A, de Roode S, Edwards J, Golaz J-C, Jiang H, Khairoutdinov M, Kirkpatrick MP, Lewellen DC, Lock A, Müller F, Stevens DE, Whelan E, Zhu P. 2005. Evaluation of large-eddy simulations via observations of nocturnal marine stratocumulus. *Mon. Weather Rev.* **133**: 1443–1462.

Tsay S-C, Jayaweera K. 1984. Physical characteristics of Arctic stratus clouds. *J. Appl. Meteorol.* **23**: 584–596.

Turner DD, Clough SA, Liljegren JC, Clothiaux EE, Cady-Pereira KE, Gaustad KL. 2007. Retrieving liquid water path and precipitable water vapor from the Atmospheric Radiation Measurement (ARM) microwave radiometers. *IEEE Trans. Geosci. Remote Sensing* **45**: 3680–3690.

Verlinde J, Harrington JY, McFarquhar GM, Yannuzzi VT, Avramov A, Greenberg S, Johnson N, Zhang G, Poellot MR, Mather JH, Turner DD, Eloranta EW, Zak BD, Prenni AJ, Daniel JS, Kok GL, Tobin DC, Holz R, Sassen K, Spangenberg D, Minnis P, Tooman TP, Ivey MD, Richardson SJ, Bahrmann CP, Shupe MD, DeMott PJ, Heymsfield AJ, Schofield R. 2007. The Mixed-Phase Arctic Cloud Experiment. *Bull. Am. Meteorol. Soc.* **88**: 205–221.

Copyright © 2009 Royal Meteorological Society

Wang Z. 2007. A refined two-channel microwave radiometer liquid water path retrieval for cold regions by using multiple-sensor measurements. *IEEE Geosci. Remote Sensing Lett.* **4**: 591–595.

Wang Z, Sassen K. 2001. Cloud type and macrophysical property retrieval using multiple remote sensors. *J. Appl. Meteorol.* **40**: 1665–1682.

Xie S, Zhang M, Branson M, Cederwall RT, Del Genio AD, Eitzen ZA, Ghan SJ, Iacobellis SF, Johnson KL, Khairoutdinov M, Klein SA, Krueger SK, Lin W, Lohmann U, Miller MA, Randall DA, Somerville RCJ, Sud YC, Walker GK, Wolf A, Wu X, Wu K-M, Yio JJ, Zhang G, Zhang J. 2005. Simulations of midlatitude frontal clouds by single-column and cloud-resolving models during the Atmospheric Radiation Measurement March 2000 cloud intensive operation period. *J. Geophys. Res.* **110**: D15S03, DOI:10.1029/2004JD005119.

Xie S, Klein SA, Zhang M, Yio JJ, Cederwall RT, McCoy R. 2006. Developing large-scale forcing data for single-column and cloud-resolving models from the Mixed-Phase Arctic Cloud Experiment. *J. Geophys. Res.* **111**: D19104, DOI:10.1029/2005JD006950.

Xu K-M, Zhang M, Eitzen ZA, Ghan SJ, Klein SA, Wu X, Xie S, Branson M, Del Genio AD, Iacobellis SF, Khairoutdinov M, Lin W, Lohman U, Randall DA, Somerville RCJ, Sud YC, Walker GK, Wolf A, Yio JJ, Zhang J. 2005. Modeling springtime shallow frontal clouds with cloud-resolving and single-column models. *J. Geophys. Res.* **110**: D15S04, DOI:10.1029/2004JD005153.

Zhu P, Bretherton CS, Köhler M, Cheng A, Chlond A, Geng Q, Austin P, Golaz J-C, Lenderink G, Lock A, Stevens B. 2005. Intercomparison and interpretation of single-column model simulations of a nocturnal stratocumulus-topped marine boundary layer. *Mon. Weather Rev.* **133**: 2741–2758.

Copyright © 2009 Royal Meteorological Society